Si_CC_{Si} antisite pairs in SiC identified as paramagnetic defects with strongly anisotropic orbital quenching

U. Gerstmann,[1,2] A. P. Seitsonen,[1] D. Ceresoli,[3] F. Mauri,[1] H. J. von Bardeleben,[4] J. L. Cantin,[4] and J. Garcia Lopez[5]
[1]*Institut de Minéralogie et de Physique des Milieux Condensés, Université Paris 6, 140 rue de Lourmel, F-75015 Paris, France*
[2]*Lehrstuhl für Theoretische Physik, Department für Naturwissenschaften, Universität Paderborn, Warburger Str. 100, D-33098 Paderborn, Germany*
[3]*Department of Materials Science and Engineering, Massachusetts Institute of Technology (MIT), 77 Massachusetts Avenue, Cambridge, Massachusetts 02139-4307, USA*
[4]*Institut des Nanosciences de Paris, Université Paris 6, 140 rue de Lourmel, F-75015 Paris, France*
[5]*Centro Nacional de Aceleradores, Thomas A. Edison, Isla de La Cartuja, E-41092 Sevilla, Spain*
(Received 8 April 2010; published 17 May 2010)

The nearest-neighbor antisite pair defects in 4H-SiC, 6H-SiC, and 3C-SiC single crystals have been identified using electron paramagnetic resonance spectroscopy in combination with a nonperturbative *ab initio* scheme for the electronic g tensor. Based on the theoretical predictions, the positively charged defect has been found experimentally also in the cubic 3C-SiC polytype where it is characterized by spin 1/2 and highly anisotropic g values of $g_{xx}=2.0030$, $g_{yy}=2.0241$, and $g_{zz}=2.0390$ within C_{1h} symmetry. The exceptional large g values are explained by details of the spin-orbit coupling causing a strongly anisotropic quenching of the orbital angular momentum of the p-like unpaired electron.

DOI: 10.1103/PhysRevB.81.195208 PACS number(s): 71.55.−i, 71.15.−m, 76.30.−v

I. INTRODUCTION

Intrinsic and irradiation induced defects in solid states have been the object of numerous experimental and theoretical studies since they influence the *electronic* properties of the materials and act as traps for intentional dopants. The basic intrinsic defects which have been clearly evidenced in many semiconductors are monovacancy and divacancy, and defect complexes related to self-interstitials, e.g., distant vacancy-interstitial pairs, so-called Frenkel pairs which are believed to be the primary irradiation-induced defects. In compound semiconductors, another important class of defects exists: the antisites. These defects, formed by atoms on the "wrong" sublattice, are quite ubiquous in the III-V compounds InP,[1] GaP,[2] and GaAs.[3] Antisites and associated complexes were *evidenced* as native defects in samples grown under nonstoichiometric conditions as well as irradiation-induced centers. Besides vacancies and some complexes related to carbon interstitials,[4–9] the antisites[10] are believed to be also quite common native defects in silicon carbide (SiC), a promising wide-gap semiconductor for high-power, high-frequency, and high-temperature electronics.[5] But, interestingly, they have escaped any convincing experimental observation in the various SiC polytypes: initial attributions to the silicon antisite Si_C have turned out to be erroneous.[9] An observation of the isolated C_{Si} antisite in the 6H-SiC has been claimed recently[11] but this attribution lacks theoretical support. A complex of a C_{Si} antisite with a carbon vacancy V_C has been reported[12] but can be regarded as a metastable state of the Si vacancy.[13] An involvement of antisite pairs Si_CC_{Si} in the omnipresent luminescent D_I center[14,15] or the so-called alphabet lines[16] was frequently discussed. The predicted too low thermal stability seems, however, to exclude this attribution.[17]

To investigate the microscopic structure of defects, electron paramagnetic resonance (EPR) is the experimental technique of choice providing a *magnetic* fingerprint of the defects including the electronic g tensor and the hyperfine (HF) splittings. The latter have been frequently decisive for the identification of defects in semiconductors. Among the irradiation-induced defects previously reported in SiC, there is one particular class of unidentified EPR centers with exceptionally anisotropic g tensors,[18,19] the so-called I,II spectra in 4H-SiC and the I,I,III spectra in 6H-SiC. Their observation in different polytypes with different doping and the fact that they are introduced by electron irradiation without any further annealing, makes a participation of dopants or residual impurities very improbable. Hence, the I,II,III spectra are expected to originate from intrinsic defects introduced by the irradiation. As no HF structure could be clearly resolved in the early reports, however, the spectra could not be attributed to any particular intrinsic defect model. From their multiplicity, they are expected to occupy all inequivalent lattice sites, the hexagonal (h) as well as the quasicubic lattice sites (k_1 and k_2 in 6H-SiC; k in 4H-SiC). In both polytypes, they have been observed with very similar principal values of the g tensor providing exceptionally large deviations up to 0.0450 from the free-electron value of $g_e=2.0023$. For intrinsic defects in SiC, this deviation is usually by an order of magnitude smaller: due to weak intrinsic spin-orbit coupling of the light elements Si and C, and because of additional quenching of the orbital angular momentum by the crystal lattice, the g values lie in the range between 1.9980 and 2.0060. Without exact knowledge of the microscopic origin, the reason for the exceptionally large g values in the case of the I,II(,III) centers has remained a mystery. An analysis of the equivalent center in 3C-SiC, that has a simpler structure with no inequivalent sites could be helpful. However, contrary to the hexagonal polytypes, intrinsic defects have been much less studied in the cubic 3C polytype where the pioneering work by Itoh *et al.*[20] has been followed by only few further investigations[21,22] so that in the 3C polytype a similar center has not been reported up to now.

In this work, we show that the defects with such large g tensors are not only observed systematically in irradiated 4H/6H-SiC but also in 3C-SiC single crystals. Based on two methods,[23,24] the latter nonperturbative one developed very recently, we present *ab initio* g-tensor calculations in the framework of density-functional theory (DFT) for a wide range of defect models. This allows us (1) to find out an optimized experimental setup to observe the corresponding EPR spectra in the cubic 3C-SiC polytype and (2) to identify these centers as positively charged antisite pairs $Si_C C_{Si}^+$ from their very particular spin Hamiltonian parameters which are shown to originate from an unusually anisotropic orbital quenching of a p-like unpaired electron.

II. EXPERIMENTS

Commercial p-type 4H and p-type 6H (0001) oriented bulk substrates and n-type free standing epitaxial (001) oriented 3C layers have been used in this study. The EPR measurements were performed with a standard X-band spectrometer at various temperatures between 4 and 300 K. Independent from the dopants, the I,II,III spectra are not observed in the as grown samples, but only after electron or proton irradiation confirming again the intrinsic nature of these defects. In the p-type doped hexagonal samples, they can be observed under thermal equilibrium conditions. In the n-type cubic layer, photoexcitation is required (see below). All defects reported here, are stable at room temperature.

A set of 4H samples have been irradiated at 77 K with electrons of various energies between 350 keV and 1 MeV at doses of 1×10^{18} e^-/cm^2. Already in the samples submitted to the lowest energy irradiation, beside the boron acceptor as a contamination of the Al-doped p-type sample and the $(C\text{-}C)_C^+$ dumbbell,[25] the I,II EPR spectra can be observed. They are characterized by a spin $S=1/2$, a point symmetry C_{1h} and quite similar, very anisotropic g tensors (Fig. 1). The principal values and the orientation of the axes relative to the crystal lattice are summarized in Table II. For some high-symmetry orientations, different HF splittings could be resolved [see Figs. 1(b) and 1(c), and Table III]. In particular, for $B\|[1100]$ we observe a strongly anisotropic HF interaction with a single Si nucleus with a maximum value of 101 MHz [see arrows in Fig. 1(c)]. For the corresponding low-field lines around 3300 G, this value is reduced to 50 MHz. For $B\|[0001]$ rather broad HF satellites with a splitting of 11 MHz and with an intensity equivalent to about two Si nuclei are observed instead.

The 3C and 6H samples have been irradiated at room temperature with a dose of $1\times10^{16}p^+/cm^2$ of high energy (6.3 MeV) protons causing a high introduction rate for primary Frenkel pairs (distant vacancy—interstitial pairs) in both, C and also Si sublattices. Both samples show under thermal equilibrium conditions a dominant spectrum of the negatively charged silicon vacancy V_{Si}^-. In the 6H crystals (p-type doped), we have equally observed the I,II,III spectra (Table II, see also Ref. 19). In the 3C-SiC samples (n-type doped), low-temperature photoexcitation with near band gap light is needed to observe an additional, very similar $S=1/2$ spectrum with C_{1h} symmetry, labeled I. The analysis of

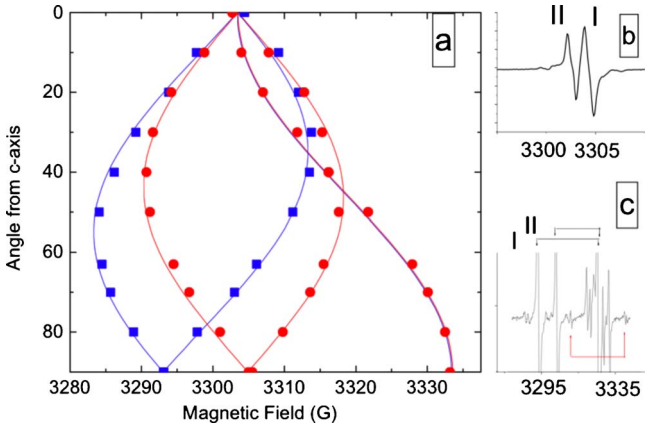

FIG. 1. (Color online) (a) Angular variation in the resonance lines of the EPR signals I (*blue squares*) and II (*red circles*) in 4H-SiC using a (11–20) rotation plane for the magnetic field. Insets: EPR spectra for $B\|[0001]$ (b) and for $B\|[1100]$ (c).

the angular variation for a rotation of the magnetic field in a (−110) plane (Fig. 2) allows us to determine its spin Hamiltonian parameters given in Table II (g tensor) and Table III (HF splittings). Independent from the direction of the magnetic field, the low-field lines are less intense and a resolution of HF splittings is not possible. For $B\|[001]$, however, we clearly resolve around the high-field line the HF interaction of 9 MHz with an intensity equivalent to about three Si nuclei (see inset of Fig. 2). Equally we observe a second set of less intense, rather broad satellite lines split by 23 MHz which can be attributed to one or two Si nuclei. HF splittings slightly below 30 MHz are also observed for the midfield (Mf_1, Mf_2) lines for $B\|[110]$ (around 3300 G). For the corresponding high-field line at 3333 G, a resolution is not possible since the EPR lines are covered by the dominant spectrum of V_{Si}^-. Most important, however, we see that the principal g values are close to those observed in the 4H and 6H polytypes (see Ref. 19, this work), strongly suggesting a common origin.

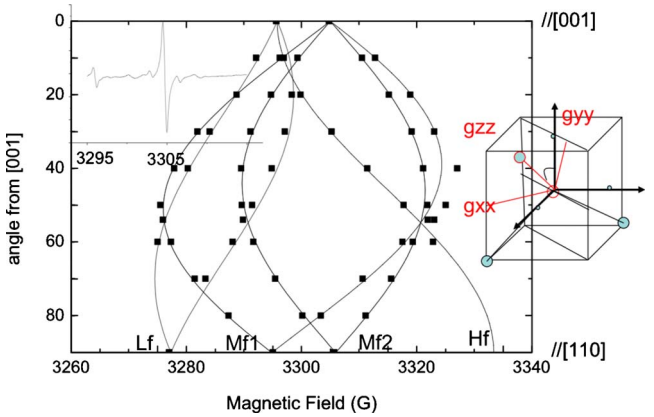

FIG. 2. (Color online) Angular variation in the resonance fields for the EPR spectrum I in 3C-SiC measured for rotating the sample in a (−110) plane. The principal g_{zz} axis includes an angle of 69° with [001] (right inset). Left inset: EPR signal for $B\|[001]$.

TABLE I. Calculated g tensors for Frenkel pairs in 3C-SiC. The values for the isolated $(C\text{-}C)_C^+$ split interstitial and V_{Si}^- are also given and compared with experimental data. ϑ is the angle between the principal axis (g_{zz}) and the [001] axis, otherwise the corresponding axis is given explicitly.

Center, model		g_{xx}	g_{yy}	g_{zz}	ϑ (°)
V_C^{2+}-$(C\text{-}C)_C^+$	C_{1h}	2.0065	2.0039	2.0009	32
V_C^{2+}-$(C\text{-}C)_C^+$	C_1	2.0031	2.0022	1.9986	19
$(C\text{-}C)_C^+$	D_2	2.0019	2.0006	1.9869	0
4H-exp (Ref. 5)	C_{1h}	2.0019	2.0015	1.9962	$(41)_{[0001]}$
$V_CC_{Si}^-$-Si_{int}^{4+}	C_{1h}	2.0041	2.0075	2.0165	85
V_{Si}^--Si_{int}^{4+}, $S=3/2$	C_{1h}	2.0022	2.0023	2.0028	65
$V_{Si}^-Si_{int}^{4+}$, $S=3/2$	C_{3v}	2.0028	2.0028	2.0031	54
$V_{Si}^-Si_{int}^{4+}$, $S=3/2$	C_{2v}	2.0029	2.0029	2.0030	0
LE1, exp (Ref. 22)	C_{2v}	2.0029	2.0029	2.0029	0
V_{Si}^-, $S=3/2$	T_d	2.0029	2.0029	2.0029	
V_{Si}^-, exp (Refs. 21 and 22)	T_d	2.0029	2.0029	2.0029	

III. COMPUTATIONAL METHOD

To find out the origin for this particular class of centers, we perform g-tensor calculations in a wide range of reasonable intrinsic defects (see Tables I and II). We use two *ab initio* methods, both implemented in the QUANTUM-ESPRESSO plane wave code:[26] the first is based on perturbation theory treating the external magnetic field as well as the spin-orbit coupling as perturbations.[23] The approach was already shown to be sufficiently precise to model quantitatively the g tensor of the carbon vacancy V_C^+ in 4H-SiC.[27]

The second method[24] allows to circumvent perturbation theory with respect to spin-orbit coupling. Instead, the Hamiltonian for the spin-orbit coupling is explicitly included in the self-consistent field calculations whereby in the

TABLE II. g tensors for Si_C-related defect models calculated via the nonperturbative method of Ref. 24. The experimental values measured in this work for the I,II,III centers (error bar ±0.0001) are also given. ϑ is the angle between the principal axis (g_{zz}) and the c axis in 4H-/6H-SiC ([001] in 3C-SiC). We emphasize in boldface the theoretical models which we assign to the observed EPR spectra.

Center, model		g_{xx}	g_{yy}	g_{zz}	ϑ (°)
3C, I	Exp.	2.0030	2.0241	2.0390	69
$(Si_C\text{-}C_{Si})^+$	**C_{1h}, *a″***	2.0049	2.0210	2.0497	64
	C_{1h}, *a′*	2.0059	2.0272	2.0591	46
Si_C^+	C_{2v}	2.0306	2.0811	2.0866	0
$(C_{Si}\text{-}Si_C\text{-}C_{Si})^+$	C_{2v}	2.0049	2.0216	2.0298	0
4H, I	Exp.	2.0030	2.0161	2.0407	63
$(Si_{C,k}\text{-}C_{Si,h})^+$	***Basal*, *a″***	2.0058	2.0278	2.0585	66
$(Si_{C,h}\text{-}C_{Si,h})^+$	*Axial*, *a′*	2.0097	2.0281	2.0697	4
$(Si_{C,k}\text{-}C_{Si,k})^+$	*Axial*, *a′*	2.0117	2.0242	2.0668	3
4H, II	Exp.	2.0029	2.0134	2.0337	52
$(Si_{C,h}\text{-}C_{Si,k})^+$	***Basal*, *a″***	2.0077	2.0225	2.0439	54
6H, I	Exp.	2.0041	2.0161	2.0407	63
$(Si_{C,k1}\text{-}C_{Si,h})^+$	***Basal*, *a″***	2.0034	2.0252	2.0507	66
6H, II	Exp.	2.0030	2.0139	2.0323	50
$(Si_{C,h}\text{-}C_{Si,k1})^+$	***Basal*, *a″***	2.0063	2.0185	2.0413	49
6H, III	Exp.	2.0023	2.0077	2.0452	66
$(Si_{C,k2}\text{-}C_{Si,k2})^+$	***Basal*, *a″***	2.0060	2.0196	2.0582	68

present implementation this is done within a collinear approximation. The deviation $\Delta g_{\mu\nu}$ from the free-electron value g_e is afterwards calculated via a spin flip within the orbital magnetization[24]—very similar to that what happens experimentally if the EPR resonance condition is fulfilled.[28] For defects in SiC with moderate deviation from the free-electron value, both methods give the same results. For example, for the isolated Si vacancy V_{Si}^{-}, both methods predict an isotropic value of $g=2.0029$ that agrees with the experimental value (see Table I). For some defects with large deviation, in contrast, the perturbative approach of Ref. 23 is unable to provide converged results even if large $8\times8\times8$ equidistant k-point meshes are used. Here, the nonperturbative method comes up to be superior yielding well-converged data for $4\times4\times4$ samplings. To model the defects, we use supercells containing 144 (6H-SiC) to 216 (3C-SiC) atoms, standard norm-conserving pseudopotentials with an energy cutoff of 50 Ry, and the spin-polarized, gradient-corrected functional of Perdew, Burke, and Ernzerhof (PBE) (Ref. 29). All defect structures have been fully relaxed using $2\times2\times2$ k-point samplings.

IV. RESULTS AND DISCUSSION

A. Electronic g tensors

We start our theoretical investigations in the cubic 3C polytype. In the irradiated samples, distant vacancy-interstitial pairs (Frenkel pairs) are believed to be the primary defects on both Si and C sublattices. For the resulting V_{Si}^{-}-$\mathrm{Si}_{\mathrm{int}}^{4+}$ and V_{C}^{2+}-$(\mathrm{C\text{-}C})_{\mathrm{C}}^{+}$ complexes, however, we calculate much too small g values (Table I) resembling those of the isolated silicon vacancy $\mathrm{V}_{\mathrm{Si}}^{-}$ (Refs. 21 and 22) and the isolated $(\mathrm{C\text{-}C})_{\mathrm{C}}^{+}$ carbon split-interstitial in 4H-SiC,[5] respectively. Note that this is true for all investigated configuration within various symmetries, i.e., this result holds independent from the relative position of the vacancy and the corresponding interstitial atom. Hence, Frenkel pairs can be excluded as an origin for the large g-value spectrum. The same is true for the isolated carbon antisite C_{Si} since it provides no paramagnetic state in the gap.

Interestingly, for a whole class of Si_{C}-including defects ($\mathrm{Si}_{\mathrm{C}}^{+}$, $\mathrm{Si}_{\mathrm{C}}\mathrm{C}_{\mathrm{Si}}^{+}$, $\mathrm{C}_{\mathrm{Si}}\mathrm{Si}_{\mathrm{C}}\mathrm{C}_{\mathrm{Si}}^{+}$) exceptionally large g values are predicted (Table II). But the orientation of the g tensor relative to the crystal lattice is only well reproduced for the *nearest-neighbor antisite pair* $\mathrm{Si}_{\mathrm{C}}\mathrm{C}_{\mathrm{Si}}^{+}$. Single positively charged, it provides an $S=1/2$ ground state within C_{1h} symmetry, whereby the unpaired electron occupies an a''-like p orbital aligned perpendicular to the mirror plane (see Fig. 3). Within C_{1h} symmetry, there exist two minima. The unpaired electron occupies either an a' or an a'' orbital, mainly localized at the Si_{C} antisite atom and one (a') or two (a'') of the in C_{3v} symmetry equivalent Si ligands (see also Fig. 5). The competing a''-like minimum provides an excited state that is calculated slightly higher in total energy. However, the orientation of its g tensor is far away from the experimentally observed value (Table II). Both, an isolated $\mathrm{Si}_{\mathrm{C}}^{+}$ as well as antisite trimers $\mathrm{C}_{\mathrm{Si}}\mathrm{Si}_{\mathrm{C}}\mathrm{C}_{\mathrm{Si}}^{+}$ (Ref. 15) provide similar magnetization densities $m(\vec{r})=n_{\uparrow}(\vec{r})-n_{\downarrow}(\vec{r})$ (mainly localized at the Si_{C} and two equivalent Si ligands). But these defects are predicted to have C_{2v} symmetry with the g tensor oriented along [001], strongly contradicting the experimental finding (Table II). From our g-tensor investigations in 3C-SiC, we can, thus, definitely confirm the antisite pair model and exclude similar antisite-related defects.

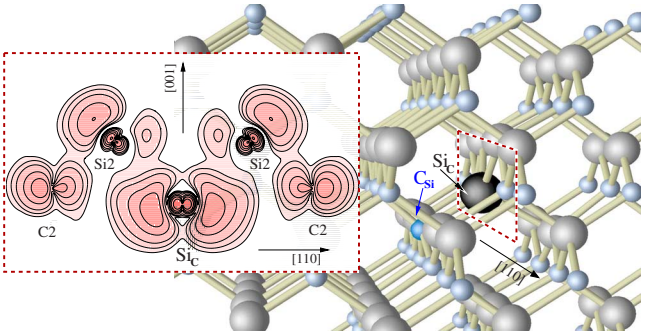

FIG. 3. (Color online) $\mathrm{Si}_{\mathrm{C}}\mathrm{C}_{\mathrm{Si}}^{+}$ antisite pair in 3C-SiC, where neighboring Si and C atoms have changed their positions. The resulting magnetization density (inset) gives rise to the EPR fingerprint of a p-like hole (see also Fig. 5) along [001].

In the hexagonal polytypes, the nearest-neighbor antisite pairs $\mathrm{Si}_{\mathrm{C}}\mathrm{C}_{\mathrm{Si}}^{+}$ may exist in axial (along the c axis) and basal configurations but only the basal antisite pairs fit the experimental results. The g tensors of the axial pairs are calculated to be slightly off-axis oriented by 4°—far away from the experimental finding (Table II). We expect that the axial pairs (and consequently also the isolated Si antisites with the largest g values) are not observable in EPR because of too fast spin-relaxation times. Hence, we attribute the two spectra in 4H-SiC and the three spectra in 6H-SiC to the positively charged basal antisite pairs with the Si_{C} antisite on the hexagonal h and quasicubic k ($k1$,$k2$) lattice sites, respectively (Fig. 4, Table II).

B. HF splittings

For antisite pairs, our *ab initio* calculations explain also nicely the observed HF structures (Table III). In the 4H samples and for basal pairs, the maximum HF splitting of

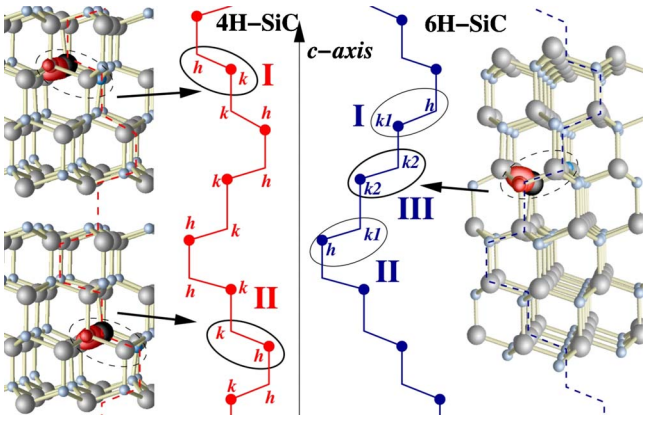

FIG. 4. (Color online) Sketch of the orientation and position of the basal antisite pairs attributed to the I,II (,III) EPR spectra in 4H-SiC and 6H-SiC. The plotted magnetization densities (red bubbles in the dashed ellipses) give rise to the EPR fingerprint. Axial pairs along the c axis are not observed.

TABLE III. Calculated hyperfine splittings (MHz) for antisite pairs in 4H-SiC and 3C-SiC. For the low-field (Lf) and high-field (Hf) lines (for B‖[110] in 3C-SiC also the midfield lines Mf_1 and Mf_2) the projections onto the direction $\vec{e}_B$ of the magnetic field B are also given and compared with experiment. For the atomic positions of the contributing nuclei, see also Fig. 3).

Model	Nuclei	A_1	A_2	A_3	$A_{\vec{e}_B}$ Lf/Hf	$\lvert A^{\exp}\rvert$ Lf/Hf	$\vec{e}_B$
4H, I	Si_C	0.0	−3.5	−97.6	−51.3/−97.6	50/99	[1100]
	Si_C				−1.6		[0001]
	$2\times Si_2$	1.5	1.0	−41.4	−1.7		[0001]
	$1\times Si_1$	8.6	7.4	6.8	8.6	11	[0001]
	$2\times C_2$	14.7	15.9	37.8	14.7	11	[0001]
4H, II	Si_C	−0.6	−3.5	−99.7	−51.6/−99.7	51/103	[1100]
	Si_C				−1.9		[0001]
	$2\times Si_2$	2.6	1.0	−42.8	−1.6		[0001]
	$1\times Si_1$	8.3	7.0	6.3	8.3	11	[0001]
	$2\times C_2$	14.7	15.9	37.8	14.7	11	[0001]
3C, I	Si_C	1.0	−2.0	−102.0	0.2/−52.0		[001]
	$2\times Si_2$	0.7	−0.1	−38.7	−8.9/−11.4	–/9	[001]
	$1\times Si_1$	6.3	7.6	8.6	7.6/7.4	–/9	[001]
	$2\times C_2$	12.3	12.4	39.5	12.9/25.9	–/23	[001]
					Mf_1/Mf_2	Mf_1/Mf_2	
	Si_C				−25.9/−25.9	29/28	[110]
	$1\times Si_2$				0.1/−23.2	29/28	[110]
	$1\times Si_2$				−23.9/0.3	29/28	[110]
	$1\times Si_1$				7.3/7.7		[110]
	$2\times C_2$				−19.3/−19.3		[110]

about 100 MHz (as predicted by our *ab initio* calculations for the Si antisite nucleus) can be observed for B‖[1100] and the high-field line belonging to the defects with a (1100) mirror plane. For other defect orientations, the magnetic field reduces the symmetry and, due to their strong anisotropy, also the HF splittings. Calculated values of −51.3 and −51.6 MHz obtained by a projection of the HF tensor onto [1100] agree exactly with the values experimentally observed for the low-field lines. For B‖[0001] the central HF splitting of the Si antisite nucleus is reduced to a value of −1.6 (I spectrum) and −1.9 MHz (II spectrum). As a result, these splittings cannot be resolved and contribute to the width of the central line instead. The analysis of the angular dependence of the central HF splitting proves that the magnetization density (determined by a a''-like electronic structure) is perfectly aligned along [1100], in other words perpendicular to the mirror plane as in the case of the I spectrum in 3C-SiC (see also Fig. 3). For the axial configurations, in contrast, the holelike unpaired electron is aligned *within* the symmetry plane (a'-like occupation) and, thus, would give rise to completely different HF parameters.[14]

Also in the 3C-SiC sample, the Si antisite nucleus is calculated to provide a maximum central HF splitting of about 100 MHz. Again, this splitting is extremely anisotropic (Table III) and depends critically on the direction of the applied magnetic field. The maximum can only be expected for the high-field line for B‖[110] (perpendicular to a symmetry plane). But here, an observation is prevented by the presence of the dominant V_{Si}^- spectra. For the two corresponding midfield lines around 3300 G, the HF splittings of the Si_C antisite nucleus as well as one of the two (in absence of the magnetic field) equivalent Si ligands are calculated to −25.9 and −23.7 MHz, respectively. They, thus, explain nicely the experimentally observed HF splitting (with two Si nuclei) slightly below 30 MHz. For B‖[001] the two Si ligands remain equivalent but according to our *ab initio* calculations their splittings are furthermore reduced to a value of −11.4 MHz. Together with the third Si ligands (within the nodal plane of the a'' orbital providing a nearly isotropic splitting around 8 MHz) they are able to explain an intensity equivalent to three Si nuclei. The HF splitting due to the Si_C antisite nucleus, in contrast, has not been clearly resolved. A theoretically predicted splitting of −52.0 MHz would coincide with the tail of the low-field EPR line at 2995 G. Since the central HF tensor is so anisotropic, however, we cannot conclusively exclude a contribution of the Si_C antisite nucleus to the 23 MHz splitting.

C. Orbital quenching and large *g*-tensor anisotropy

The anisotropic shape of the magnetization density resembling that of a *p*-like hole (see inset of Figs. 3 and 5) is also

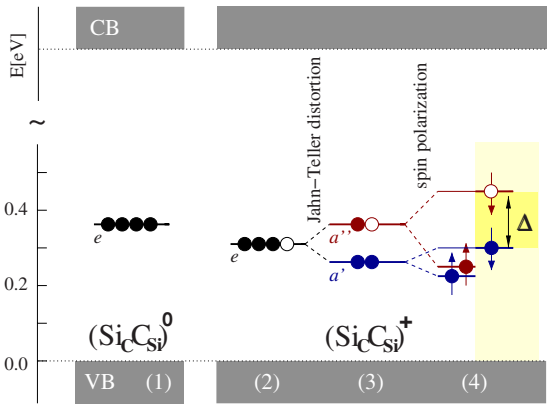

FIG. 5. (Color online) Sketch of the one-particle levels for the antisite pair in 3C-SiC: (1) for the neutral charge state (C_{3v} symmetry) the dominant levels of the irreducible representation e are degenerate. (2) For $Si_C C_{Si}^+$ a "hole" arises in the e level. The potential becomes more attractive, lowering the energetic position of the e level. (3) Occupied with three electrons, the electronic configuration is Jahn-Teller instable, lowering the symmetry toward C_{1h} and splitting up the e level in two nondegenerate levels (a' and a''). (4) Spin polarization enhances the HOMO-LUMO gap Δ in the spin-down channel, whereby Δ determines the orbital quenching.

the basic key to explain the exceptionally large g values. Defects in solids usually show a large degree of orbital quenching in any direction, especially in covalently bound semiconductors. For the antisite pairs in SiC, in contrast, the orbital quenching is extremely anisotropic: parallel to the p-like hole, the orbital angular momentum is suppressed completely ($g_{xx} \approx g_e$, see Table II). For the other two principal axes perpendicular to the hole [both lying in the (110) mirror plane of the defect], the g tensor can well be presented as $g_{yy}=g_e+\frac{\lambda}{\Delta}$ and $g_{zz}=g_e+2\frac{\lambda}{\Delta}$, similar to tetragonal systems in ionic crystals.[28] Here, λ denotes the spin-orbit coupling constant and Δ is the gap between the highest-occupied molecular orbital (HOMO) and lowest-unoccupied molecular orbital (LUMO) in the minority spin channel, mediating the orbital quenching of the holelike electronic configuration. In the case of an antisite pair, this gap is opened due to the Jahn-Teller distortion toward C_{1h} symmetry (crystal-field splitting), whereby the spin polarization yields to a considerable enhancement of this value (for, e.g., 3C-SiC, see Fig. 5).[30] In Table IV, we have collected the *effective* spin-orbit coupling constants $\lambda=\Delta\cdot\frac{1}{3}\mathrm{Tr}(\Delta g)$ derived from the k-point averaged[31] HOMO-LUMO gap Δ and the trace of $g-g_e$ as obtained by our *ab initio* calculations. For the V_C-related defects with Si dangling bond-like (sp^3-hybridized) unpaired electrons, the values are about two orders of magnitude smaller if compared with the 149 cm^{-1} for an ionized Si^+ atom.[32] For all Si_C-including centers, in contrast, we obtain spin-orbit coupling constants λ that are only moderately reduced in comparison with the atomic value showing a minor influence of the crystal lattice. This, in semiconductors unusual effect of more or less *crystal-field independent* orbital quenching is also manifested in the perfect p-like alignment of the magnetization density perpendicular to the symmetry plane (Fig. 3), and gives rise to the extremely anisotropic shape of the HF splittings (see Sec. IV B).

D. Defect formation

We will now discuss possible formation mechanisms of the antisite pair defect. During the diffusion process of ions, the antisite pair can be easily formed.[33] Its observation in low-energy electron-irradiated 4H-SiC is, however, *a priori* surprising as carbon Frenkel pairs are the expected dominant defects. If the energy is not sufficient to remove a Si atom completely from its lattice site, a tilted structure in which the Si interstitial is stabilized by a C_{Si} antisite (left part of Fig. 6) is predicted by our DFT calculations. In analogy to distant Si

TABLE IV. Analysis of the calculated g tensors: spin-orbit coupling constants $\lambda=\Delta\cdot\frac{1}{3}\mathrm{Tr}(\Delta g)$ derived from the trace of $g-g_e$ and the k-point averaged energy gap $\Delta=\frac{1}{N_k}\Sigma_k\Delta_k$.

Polytype	Center	Model		$\frac{1}{3}\mathrm{Tr}(\Delta g)$	Δ (eV)	λ (cm^{-1})
3C		V_C^{2+}-$(C\text{-}C)_C^+$	C_1	0.0010	0.656	5.3
3C		$V_C C_{Si}^-$-Si_{int}^{4+}	C_{1h}	0.0049	0.228	9.0
3C		$(Si_C\text{-}C_{Si})^+$	C_{1h}, a''	0.0299	0.169	31.1
3C	I	Si_C^+	C_{2v}	0.0638	0.080	41.2
3C		$(C_{Si}\text{-}Si_C\text{-}C_{Si})^+$	C_{2v}	0.0165	0.325	43.2
3C		$(Si_{C,h}\text{-}C_{Si,h})^+$	*Axial*, a'	0.0335	0.182	47.8
3C		$(Si_{C,k}\text{-}C_{Si,k})^+$	*Axial*, a'	0.0326	0.164	43.0
4H	I	$(Si_{C,k}\text{-}C_{Si,h})^+$	*Basal*, a''	0.0284	0.191	43.6
4H	II	$(Si_{C,h}\text{-}C_{Si,k})^+$	*Basal*, a''	0.0224	0.211	38.1
6H	I	$(Si_{C,k1}\text{-}C_{Si,h})^+$	*Basal*, a''	0.0413	0.181	35.2
6H	II	$(Si_{C,h}\text{-}C_{Si,k1})^+$	*Basal*, a''	0.0197	0.196	31.2
6H	III	$(Si_{C,k2}\text{-}C_{Si,k2})^+$	*Basal*, a''	0.0256	0.191	39.3

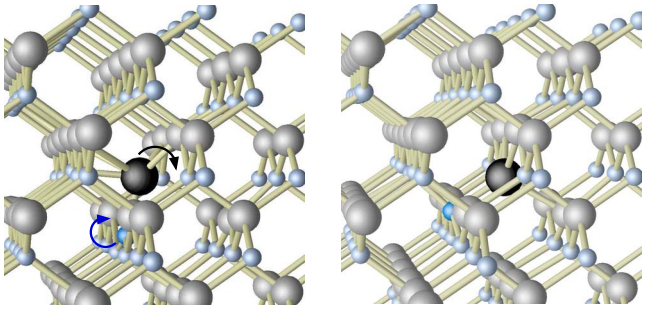

FIG. 6. (Color online) $V_CC_{Si}^{-}$-Si_{int}^{4+} complex (left) as an initial stage for an antisite pair (right) in 3C-SiC (large balls denote Si atoms, small balls C atoms). The initial complex can be formed if the energy is too low to create a distant Si-Frenkel pair. The arrows describe the barrier-free formation path toward the antisite pair $(Si_CC_{Si})^+$ (after electron capture).

Frenkel pairs, the resulting $V_CC_{Si}^{-}$-Si_{int}^{4+} complex is initially threefold positively charged (in total). Like the Frenkel pairs, however, this complex itself can by no means explain the observed EPR spectra: the deviations of g_{zz} and g_{yy} from the free-electron value g_e are much too small (see also Table I). After capture of two electrons, the resulting singly positive charge state is in DFT unstable and relaxes *without any barrier* into the nearest-neighbor antisite pair $(Si_CC_{Si})^+$ (Fig. 6). From our results it can, however, not be excluded that the antisite pairs could also be native defects which are transformed into a paramagnetic charge state by the electrical compensation accompanying the irradiation.

V. SUMMARY

In this work, the application of a theoretical *ab initio* approach[24] has allowed us to identify antisite pair defects in SiC from their very particular g tensors. The exceptionally large deviations from the free-electron-value g_e, very unusual for intrinsic defects, are shown to originate from an anisotropic quenching of the orbital angular momentum of a p-like hole. By this, remaining doubts concerning the intrinsic character of the responsible defects have been conclusively removed. The antisite pair defects have been detected in various polytypes after electron and proton irradiation, independent from the type of doping and independent from the energy of the irradiation. We have presented a low-energy scenario for the defect formation where the antisite pairs are generated if the irradiation energies are too low to create distant Si-Frenkel pair. Since they can also be easily formed during growth or during the diffusion process of ions, and since they can be observed in all types of samples, the antisite pairs are believed to be one of the major defects, if the material is not exposed to too high annealing temperatures.[17]

In the hexagonal polytypes, the multiplicity of the spectra is explained by basal antisite pairs with the silicon antisite atom at the inequivalent hexagonal and quasicubic lattice sites. The axial pairs have not been observed, most probably due to too short spin-relaxation times. Also taking into account the presence of basal and axial pairs, a complete averaging of the magnetic anisotropy over the different orientations is prevented. Thus, in hexagonal samples with a high amount of paramagnetic antisite pairs, the reported anisotropic orbital quenching should result in anisotropic macroscopic magneto-optical properties of the material.

ACKNOWLEDGMENTS

U.G. is grateful to acknowledge financial support by the DFG (Grant No. GE 1260/3-1) and by the CNRS. The calculations were performed at the IDRIS supercomputing center in Paris-Orsay (Grant No. 061202).

[1] D. Y. Jeon, H. P. Gislason, J. F. Donegan, and G. D. Watkins, Phys. Rev. B **36**, 1324 (1987).
[2] B. K. Meyer and J.-M. Spaeth, Phys. Rev. B **32**, 1409 (1985).
[3] H. Overhof and J. M. Spaeth, Phys. Rev. B **72**, 115205 (2005).
[4] M. E. Zvanut and J. Phys. C: Condens. Matter **16**, R1341 (2004).
[5] N. T. Son, Mt. Wagner, C. G. Hemmingsson, L. Storasta, B. Magnusson, W. M. Chen, S. Greulich-Weber, J. M. Spaeth, and E. Janzén, in *Silicon Carbide—Recent Major Advances*, edited by W. J. Choyke, H. Matsunami, and G. Pensl (Springer, New York, 2004), p. 461–488.
[6] E. Janzén, N. T. Son, B. Magnusson, and A. Ellison, Microelectron. Eng. **83**, 130 (2006).
[7] J. Isoya, T. Umeda, N. Mizuochi, N. T. Son, E. Janzén, and T. Oshima, Phys. Status Solidi B **245**, 1298 (2008).
[8] M. Bockstedte, A. Gali, A. Mattausch, O. Pankratov, and J. W. Steeds, Phys. Status Solidi B **245**, 1281 (2008).
[9] N. T. Son, P. N. Hai, and E. Janzén, Phys. Rev. Lett. **87**, 045502 (2001).
[10] L. Torpo, S. Pöykkö, and R. M. Nieminen, Phys. Rev. B **57**, 6243 (1998).
[11] P. G. Baranov, I. V. Ilyin, A. A. Soltamova, and E. N. Mokhov, Phys. Rev. B **77**, 085120 (2008).
[12] T. Umeda, N. T. Son, J. Isoya, E. Janzen, T. Ohshima, N. Morishita, H. Itoh, A. Gali, and M. Bockstedte, Phys. Rev. Lett. **96**, 145501 (2006).
[13] E. Rauls, T. Lingner, Z. Hajnal, S. Greulich-Weber, T. Frauenheim, and J.-M. Spaeth, Phys. Status Solidi B **217**, R1 (2000).
[14] A. Gali, P. Deák, E. Rauls, N. T. Son, I. G. Ivanov, F. H. C. Carlsson, E. Janzén, and W. J. Choyke, Phys. Rev. B **67**, 155203 (2003); Physica B **340-342**, 175 (2003).
[15] M. V. B. Pinheiro, E. Rauls, U. Gerstmann, S. Greulich-Weber, H. Overhof, and J.-M. Spaeth, Phys. Rev. B **70**, 245204 (2004).
[16] T. A. G. Eberlein, R. Jones, S. Öberg, and P. R. Briddon, Phys. Rev. B **74**, 144106 (2006).
[17] M. Posselt, F. Gao, and W. J. Weber, Phys. Rev. B **73**, 125206 (2006).
[18] D. Cha, H. Itoh, N. Morishita, A. Kawasuso, T. Ohshima,

Y. Watanabe, J. Ko, K. Lee, and I. Nashiyama, Mater. Sci. Forum **264-268**, 615 (1998).
[19] N. T. Son, P. N. Hai, P. T. Huy, T. Gregorkiewicz, C. A. J. Ammerlaan, J. L. Lindström, W. M. Chen, B. Monemar, and E. Janzén, Physica B **273-274**, 655 (1999).
[20] H. Itoh, A. Kawasuso, T. Ohshima, M. Yoshikawa, I. Nashiyama, S. Tanigawa, S. Misawa, H. Okumura, and S. Yoshida, Phys. Status Solidi A **162**, 173 (1997).
[21] T. Wimbauer, B. K. Meyer, A. Hofstaetter, A. Scharmann, and H. Overhof, Phys. Rev. B **56**, 7384 (1997).
[22] N. T. Son, E. Janzén, J. Isoya, N. Morishita, H. Hanaya, H. Takizawa, T. Ohshima, and A. Gali, Phys. Rev. B **80**, 125201 (2009).
[23] Ch. J. Pickard and F. Mauri, Phys. Rev. Lett. **88**, 086403 (2002); Phys. Rev. B **63**, 245101 (2001).
[24] D. Ceresoli, U. Gerstmann, A. P. Seitsonen, and F. Mauri, Phys. Rev. B **81**, 060409(R) (2010).
[25] T. Petrenko, T. L. Petrenko, and V. Ya Bratus, J. Phys.: Condens. Matter **14**, 12433 (2002).
[26] P. Giannozzi, S. Baroni, N. Bonini, M. Calandra, R. Car, C. Cavazzoni, D. Ceresoli, G. L. Chiarotti, M. Cococcioni, I. Dabo, A. D. Corso, S. de Gironcoli, S. Fabris, G. Fratesi, R. Gebauer, U. Gerstmann, C. Gougoussis, A. Kokalj, M. Lazzeri, L. Martin-Samos, N. Marzari, F. Mauri, R. Mazzarello, S. Paolini, A. Pasquarello, L. Paulatto, C. Sbraccia, S. Scandolo, G. Sclauzero, A. P. Seitsonen, A. Smogunov, P. Umari, and R. M. Wentzcovitch, J. Phys.: Condens. Matter **21**, 395502 (2009); http://www.quantum-espresso.org
[27] U. Gerstmann, A. P. Seitsonen, F. Mauri, and H. J. von Bardeleben, Mater. Sci. Forum **615-617**, 357 (2009).
[28] J. M. Spaeth and H. Overhof, *Point Defects in Semiconductors and Insulators* (Springer, New York, 2003).
[29] J. P. Perdew, K. Burke, and M. Ernzerhof, Phys. Rev. Lett. **78**, 1396 (1997).
[30] The trend of overestimated Δg values for the Si_C-related defects is attributed (1) to the used DFT functionals as they provide too low-lying empty states (too small "gaps" Δ) and underestimated crystal-field splittings and (2) to uncertainties in the description of the spin splitting, e.g., those introduces by the usual collinear approximation.
[31] Due to limited supercell sizes, an artificial dispersion of the levels in the fundamental gap is unavoidable. We take into account this effect by presenting values averaged over the *k*-point samplings (in Table IV and also in Fig. 5).
[32] W. R. Wadt, Chem. Phys. Lett. **89**, 245 (1982).
[33] E. Rauls, M. V. B. Pinheiro, S. Greulich-Weber, and U. Gerstmann, Phys. Rev. B **70**, 085202 (2004).